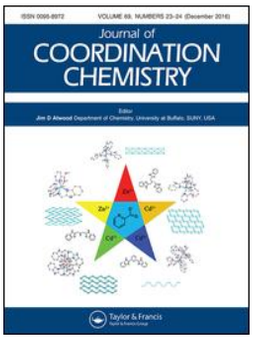

Journal of Coordination Chemistry

ISSN: 0095-8972 (Print) 1029-0389 (Online) Journal homepage: www.tandfonline.com/journals/gcoo20

Octahedral iron(II) complexes with pyridyl triazine and bipyridine ligands – synthesis, computational studies, mechanisms and kinetics with 1,10-phenanthroline and 2,2',6,2"-terpyridine

Rajesh Bellam, Surapureddy Sivamadhavi, Saladi Ramakrishna, Allen Mambanda, Deogratius Jaganyi & Nageswararao Anipindi

To cite this article: Rajesh Bellam, Surapureddy Sivamadhavi, Saladi Ramakrishna, Allen Mambanda, Deogratius Jaganyi & Nageswararao Anipindi (2017) Octahedral iron(II) complexes with pyridyl triazine and bipyridine ligands – synthesis, computational studies, mechanisms and kinetics with 1,10-phenanthroline and 2,2',6,2"-terpyridine, Journal of Coordination Chemistry, 70:11, 1893-1909, DOI: 10.1080/00958972.2017.1324954

To link to this article: https://doi.org/10.1080/00958972.2017.1324954

JOURNAL OF COORDINATION CHEMISTRY, 2017
VOL. 70, NO. 11, 1893–1909
https://doi.org/10.1080/00958972.2017.1324954

Taylor & Francis
Taylor & Francis Group

Octahedral iron(II) complexes with pyridyl triazine and bipyridine ligands – synthesis, computational studies, mechanisms and kinetics with 1,10-phenanthroline and 2,2′,6,2″-terpyridine

Rajesh Bellam[a,b], Surapureddy Sivamadhavi[b], Saladi Ramakrishna[b,c], Allen Mambanda[a], Deogratius Jaganyi[a] and Nageswararao Anipindi[b]

[a]School of Chemistry and Physics, University of KwaZulu-Natal, Pietermaritzburg, South Africa; [b]Department of Physical and Nuclear Chemistry and Chemical Oceanography, Andhra University, Visakhapatnam, India; [c]Department of Chemistry, Adikavi Nannaya University, Rajamahendravaram, India

ABSTRACT

[Bis(3-(2-pyridyl)-5,6-diphenyl-1,2,4-triazine)(2,2′-bipyridine)iron(II)], $[Fe(PDT)_2(bpy)]^{2+}$ (**1**), [bis(3-(4-phenyl-2-pyridyl)-5,6-diphenyl-1,2,4-triazine)(2,2′-bipyridine)iron(II)], $[Fe(PPDT)_2(bpy)]^{2+}$ (**2**), [bis(2,2′-bipyridine)(3-(2-pyridyl)-5,6-diphenyl-1,2,4-triazine)iron(II)], $[Fe(PDT)(bpy)_2]^{2+}$ (**3**), and [bis(2,2′-bipyridine)(3-(4-phenyl-2-pyridyl)-5,6-diphenyl-1,2,4-triazine)iron(II)], $[Fe(PPDT)(bpy)_2]^{2+}$ (**4**) have been synthesized and characterized. Substitution of the triazine and bipyridine ligands from the complexes by nucleophiles (nu), namely 1,10-phenanthroline (phen) and 2,2′,6,2″-terpyridine (terpy) was studied in a sodium acetate-acetic acid buffer over the pH range 3–6 at 25, 35, and 45°C under *pseudo*-first order conditions. Reactions are first order in the concentration of complexes **1**–**4**. The reaction rates increase with increasing [nu] and pH whereas ionic strength has no effect on the rate. Straight-line plots with positive slopes are observed when the k_{obs} values are plotted against [nu] or $1/[H^+]$. The substitution reactions proceed by dissociative as well as associative paths and the latter path is predominant. Observed low E_a values and negative $\Delta S^{\#}$ values support the dominance of the associative path. Phenyl groups on the triazine ring modulate the reactivity of the complexes. The π-electron cloud on the phenyl rings stabilizes the charge on metal center by inductive donation of electrons toward the metal center, resulting in a decrease in reactivity of the complex and the order is **1** < **2** < **3** < **4**. Density functional theory (DFT) calculations also support the interpretations drawn from the kinetic data.

ARTICLE HISTORY
Received 19 August 2016
Accepted 9 April 2017

KEYWORDS
Octahedral iron(II) complexes; PDT; PPDT; DFT; phen; terpy; substitution; dissociative; associative; mechanism; basicity

CONTACT Rajesh Bellam rajeshchowdarybellam@gmail.com
Supplemental data for this article can be accessed at https://doi.org/10.1080/00958972.2017.1324954.

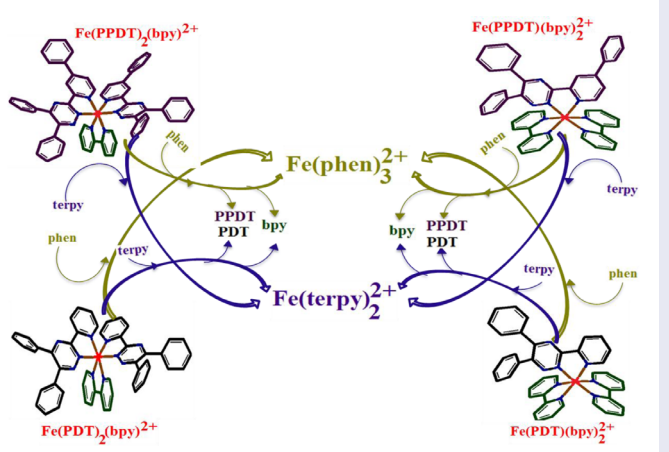

1. Introduction

Polypyridyl ligands like 1,10-phenanthroline (phen), 2,2′-bipyridine (bpy), 2,2′,6,2″-terpyridine (terpy) and substituted pyridyl triazines form thermodynamically stable 5-membered chelates with most transition metals ions (*e.g.* Fe(II), Cu(II) and Ru(II)) [1–6]. The aromatic α,α′-diimine bonds endow the complexes with high molar absorptivities which make them attractive probes for photophysical applications. For example, substituted pyridyl-triazines such as 3-(2-pyridyl)-5,6-diphenyl)-1,2,4-triazine (PDT) [7, 8] and 3-(4-phenyl-2-pyridyl)-5,6-diphenyl)-1,2,4-triazine (PPDT) [9, 10] give intense-colored octahedral iron(II) complexes, $[Fe(PDT)_3]^{2+}$ ($\lambda_{max} = 555$ nm, $\varepsilon_{max} = 2.35 \times 10^4\ M^{-1}\ cm^{-1}$) and $[Fe(PPDT)_3]^{2+}$ ($\lambda_{max} = 564$ nm, $\varepsilon_{max} = 2.87 \times 10^4\ M^{-1}\ cm^{-1}$), respectively.

Several reports appear in the literature on the solution chemistry of octahedral iron(II) complexes containing mixed-polypyridyl ligands. Schilt *et al*. [11] prepared and characterized the octahedral mixed-ligand complexes of iron(II)/iron(III) with cyanide and aromatic di-imine ligands. Later Schilt in collaboration with Taylor [12] prepared Fe(II) mixed-ligand complexes of the type $[Fe(phen)_nL_{3-n}]X_2$ and $[Fe(terpy)(TPTZ)]X_2$ (where $n = 1$ or 2, L = methyl-, phenyl-, nitro- or chloro-substituted phen and X = perchlorate or iodide ion). Burgess and co-workers [13] reported on the mechanistic aspects of the formation of [iron(II)(cyanide)(phen)] and related complexes. Also reported in the literature are Fe(II) complexes of the type $[FeL_2X_2]^{2+}$ and $[FeLX_4]^{2+}$, where L = phen or bpy and X = cyanide or oxalate ion [14–17] and $[Fe(L)(L')_2]^{2+}$ and $[Fe(L)_2(L')]^{2+}$ (L = phen, L′ = phen-5,6-dione or 4,7-dimethyl-phen) [18, 19]. Most mixed-ligand complexes of iron(II) have been made mainly for DNA-binding studies [19–22]. There are no reports on the substitution kinetics of the octahedral Fe(II) complexes with polypyridyl ligands. We have synthesized and characterized the mixed-ligand complexes of iron(II) containing pyridyl triazine (PDT/PPDT) and bipyridine ligands, $[Fe(PDT)_2(bpy)]^{2+}$ (**1**), $[Fe(PPDT)_2(bpy)]^{2+}$ (**2**), $[Fe(PDT)(bpy)_2]^{2+}$ (**3**)

and $[Fe(PPDT)(bpy)_2]^{2+}$ (**4**). We report on the kinetic and mechanism of substitution reactions of complexes **1**–**4** with phen and terpy in an acetate buffer in the pH range 3–6. We undertook this work to understand the reactivity order of the complexes towards the polypyridyl nucleophiles.

2. Experimental

2.1. Reagents and apparatus

Phen, terpy, bpy, iron(II) sulfate heptahydrate, and sodium iodide (Sigma Aldrich) and PDT and PPDT (GFS Chemicals Inc., USA) were used without further purification. Solutions of phen (0.01 M in 0.01 M HNO_3) and terpy (0.01 M in methanol) were prepared by dissolving requisite quantities. Acetate buffers of pH between 3.5 and 6.0 were prepared by mixing stoichiometric amounts of acetic acid (1.0 M) and sodium acetate (1.0 M). All these reagents were stored in amber-colored bottles. Electron-spray ionization (ESI) mass spectra of the complexes were recorded on a Waters TOF Micro-mass LCT Premier Spectrometer operated in the positive ion mode. Elementary composition of the complexes was determined on a Flash 2000 Thermo Scientific CHNS-O Analyser. The elementary composition of Fe in complexes **1**–**4** was determined spectrophotometrically after a nitric digestion step. The triazine ligand 3-(2-pyridyl)-5,6-bis(4-phenyl-sulfonic acid)-1,2,4-triazine, PDTS forms an intense-colored 1:3 complex with iron(II), $[Fe(PDTS)_3]^{4-}$ (λ_{max} = 562 nm and $\varepsilon_{max} = 2.79 \times 10^4\ M^{-1}\ cm^{-1}$) [2, 23]. 0.05 g of **1**/**2**/**3**/**4** was digested with 10 mL of 50% HNO_3 until all the organic matter was destroyed, followed by dilution to 100 mL. PDTS was then added in excess to quantitatively form $[Fe(PDTS)_3]^{4-}$. The concentration of the resultant $[Fe(PDTS)_3]^{4-}$ was determined at 562 nm and the results were used to estimate the elementary composition of Fe for each complex. UV–vis spectra and kinetic measurements of slow reactions were recorded on a Varian Cary 100 Bio UV–vis spectrophotometer with a cell compartment thermostated by a Varian Peltier temperature controller with an accuracy of ± 0.05°C.

2.2. Preparation of mixed ligand complexes

The Fe(II) complexes were prepared according to the procedure of Taylor and Schilt [12]. Requisite equivalents (PDT / PPDT (1.0 mmol) and bpy (0.5 mmol) for **1** and **2** or PDT / PPDT (0.5 mmol) and bpy (1.0 mmol) for **3** and **4**) were dissolved in 20 mL of hot ethyl alcohol. A solution of iron(II) sulfate heptahydrate (0.139 g, 0.50 mmol) in 5 mL of ultrapure water was added drop-by-drop with continuous stirring. The resultant solution was evaporated to 20 mL and filtered by Millipore micro filter paper. Filtrate was cooled to room temperature and a slight excess of sodium iodide (0.3 g) dissolved in 2 mL of water added to it in drops. The resultant solution was cooled at –5°C for about 2 h and the precipitate which was formed was separated by suction and washed several times with 5-mL aliquots of ice water and diethylether before drying under vacuum. Mass and elemental analysis data are given in table 1 and the mass spectra for complexes are given as Supplementary Data. The structures of complexes **1**–**4** are shown in scheme 1 and the visible absorption spectra are given as Supplementary Data.

Table 1. Mass and elemental analysis data of iron(II) complexes **1**–**4**.

Complex / molecular formula		Yield	ESI-MS: *m/z* (%)	Elemental analysis	
				Calc.	Found
(**1**)	$[Fe(PDT)_2(bpy)]I_2{\cdot}H_2O$	454 mg (86%)	493.16 (M^+ –I, PDT, bpy100%)	C, 54.37;	C, 54.32;
	($C_{50}H_{36}N_{10}FeI_2{\cdot}H_2O$)		416.14 (M^{2+} –I_2, 55%)	H, 3.47;	H, 2.90;
				N, 12.68;	N, 12.65;
				O, 1.45;	O, 1.41;
				Fe, 5.06	Fe, 4.92
(**2**)	$[Fe(PPDT)_2(bpy)]$	532 mg (88%)	725.11 (M^+ –I, PPDT78%)	C, 59.68;	C, 60.01;
	$I_2{\cdot}0.5H_2O$				
	($C_{62}H_{44}N_{10}FeI_2{\cdot}0.5H_2O$)		492.18 (M^{2+} –I_2, 100%)	H, 3.64;	H, 3.73;
				N, 11.23;	N, 11.19;
				O, 0.64;	O, 0.88;
				Fe, 4.48	Fe,4.43
(**3**)	$[Fe(PDT)(bpy)_2]I_2{\cdot}H_2O$	355 mg (79%)	803.72 (M^+ –I, 80%)	C, 50.55;	C, 50.68;
	($C_{40}H_{30}N_8FeI_2{\cdot}H_2O$)		649.24 (M^+ –I, bpy60%)	H, 3.39;	H, 3.17;
			399.15 (M^{2+} –I_2, 100%)	N, 11.79;	N, 11.99;
				O, 1.68;	O, 1.82;
				Fe, 5.88	Fe, 5.87
(**4**)	$[Fe(PPDT)(bpy)_2]I_2$	396 mg (81%)	754.19 (M^+ –I_2, 70%)	C, 54.79;	C, 54.71;
	($C_{46}H_{34}N_8FeI_2$)		377.78 (M^{2+} –I_2, 100%)	H, 3.40;	H, 3.19;
				N, 11.11;	N, 10.78;
				Fe, 5.54	Fe, 5.51

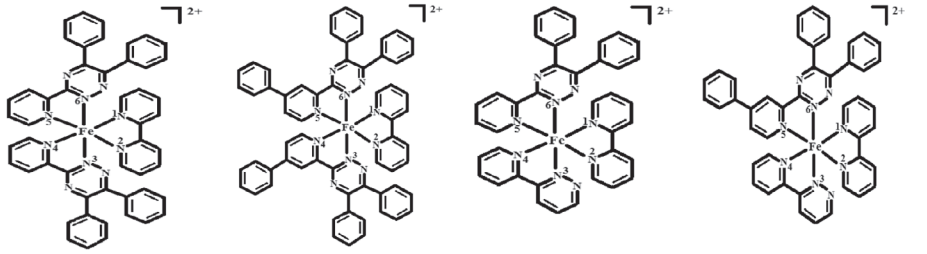

Scheme 1. The structures of the complexes $[Fe(PDT/PPDT)_{3-x}(bpy)_x]^{2+}$, x =1 or 2.

2.3. Product analysis

Requisite mass or volume of complex, nu, acetic acid/sodium acetate buffer, and sodium nitrate were transferred into amber-colored 10-mL volumetric flasks and the contents were made up to the mark with water. These solutions were left to stand for sufficient time to allow the reaction to complete (about 96 h). The UV–vis absorption spectra of the solutions after a complete substitution of complexes **1**–**4** by phen or terpy were recorded. Absorption spectra of the substitution products of complexes **1**–**4** with phen and terpy show common absorption peaks at 510 nm (ε_{max} = 11,050 ± 50 M^{-1} cm^{-1}) and at 552 nm (ε_{max} = 12,400 ± 90 M^{-1} cm^{-1}), respectively. These characteristic absorption peaks are due to $[Fe(phen)_3]^{2+}$ (for reactions with phen) and $[Fe(terpy)_2]^{2+}$ (for reactions with terpy), respectively. The spectra are given in figure 1. The molar absorptivities of the products at 510 nm and 552 nm were calculated on the basis of the concentration of iron(II) corresponding to that of $[Fe(phen)_3]^{2+}$ and $[Fe(terpy)_2]^{2+}$, respectively.

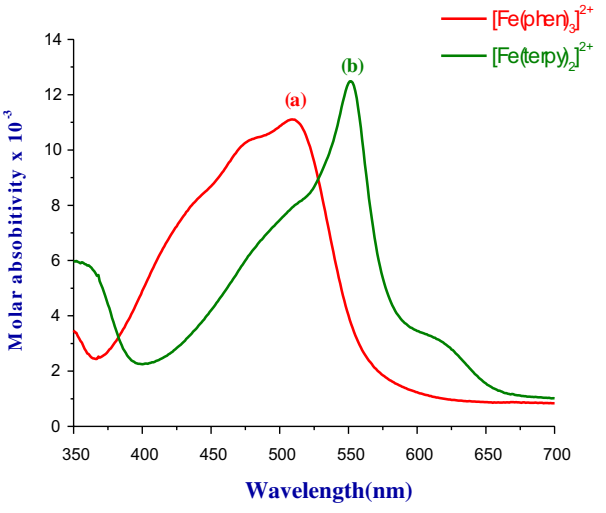

Figure 1. UV–vis absorption spectra of the reaction products of complexes **1**–**4** with (a) phen and (b) terpy.

2.4. Kinetic procedure

Kinetic runs were performed spectrophotometrically by monitoring the absorbance changes at λ_{max} values of complexes **1**–**4** as a function of time using a Cary 100 Bio UV–vis spectrophotometer. The spectral changes were recorded over the wavelength range from 350 to 700 nm. All kinetic runs were performed under pseudo-first order conditions with [nu] over the [complex] in at least 15-fold excess. The absorbance changes were followed up to eight half-lives. The effect of [complex] on the reaction rate was studied by carrying out kinetic runs at different concentrations of complex ($0.5–4.0 \times 10^{-5}$ M) at pH = 4.0, $\mu = 0.1$ mol dm^{-3} and [nu] at 1.0×10^{-3} M. The reactions were also carried out at various concentrations of phen/terpy ranging from $0.5–3.0 \times 10^{-3}$ M and variable pH within the range 3–6. The kinetic runs were also performed at 25, 35, and 45°C to study the effect of temperature on the rate of these reactions. The Origin 7.5® graphical analysis software [24] was used to obtained the *pseudo*-first-order rate constants (k_{obs}). The absorbance-time data at λ_{max} was fit to a non-linear least-square single exponential function $A_t = A_\infty + (A_o - A_\infty)\exp^{(-k_{obs}t)}$, where A_o, A_t, and A_∞ represent the absorbance of the reaction mixture initially, at time t and at the end of the reaction, respectively. All kinetic traces fitted perfectly to a single exponential function and the values of k_{obs} were reproducible to within ± 6%. A summary of the observed *pseudo*-first-order rate constant, k_{obs} at different concentrations of complex and nu, pH, and ionic strength (μ) is reported in table 2. The spectral changes accompanying the reactions were monitored at 554 nm ($\varepsilon_{max} = 18{,}500 \pm 50$ M^{-1} cm^{-1}), 564 nm ($\varepsilon_{max} = 21{,}900 \pm 80$ M^{-1} cm^{-1}), 552 nm ($\varepsilon_{max} = 13{,}600 \pm 90$ M^{-1} cm^{-1}), and 560 nm ($\varepsilon_{max} = 15{,}400 \pm 60$ M^{-1} cm^{-1}) for complexes **1**–**4**, respectively. Figure 2 shows spectral changes for the substitution of $[Fe(PDT)_2(bpy)]^{2+}$ by phen and the inset is a kinetic trace of the time dependence of the absorbance at 554 nm. The UV–vis spectra of **1**–**4** are given as Supplementary Data.

Table 2. k_{obs} values for the substitution of complexes **1**–**4** by phen and terpy at 35°C.

				$k_{obs} \times 10^4$, (M)							
				phen				terpy			
pH	nu	C	μ	**1**	**2**	**3**	**4**	**1**	**2**	**3**	**4**
3.6	1.0	2.0	0.2	5.31	6.69	9.75	11.26	5.31	6.67	9.70	11.20
4.0	1.0	2.0	0.2	5.41	6.80	10.01	11.61	5.38	6.76	9.88	11.46
4.4	1.0	2.0	0.2	5.71	7.09	10.65	12.49	5.55	6.97	10.34	12.11
4.8	1.0	2.0	0.2	6.06	7.82	12.27	14.69	5.97	7.52	11.49	13.73
5.2	1.0	2.0	0.2	7.57	9.66	16.33	20.21	7.05	8.90	14.37	17.82
5.6	1.0	2.0	0.2	10.59	14.26	26.52	34.10	9.74	12.35	21.61	28.07
4.0	0.5	2.0	0.2	5.35	6.71	10.03	11.66	5.32	6.69	9.73	11.33
4.0	1.5	2.0	0.2	5.46	6.90	10.86	12.82	5.43	6.84	10.04	12.02
4.0	2.0	2.0	0.2	5.58	6.69	11.34	13.40	5.48	6.91	10.21	12.36
4.0	2.5	2.0	0.2	5.62	7.09	11.67	13.98	5.54	6.98	10.34	12.71
4.0	3.0	2.0	0.2	5.71	7.18	12.06	14.56	5.60	7.06	10.48	13.05
4.0	1.0	0.5	0.2	5.40	7.00	9.93	11.52	5.40	6.76	9.77	11.31
4.0	1.0	1.0	0.2	5.51	6.87	10.17	11.64	5.26	6.59	9.87	11.41
4.0	1.0	1.5	0.2	5.34	6.91	10.11	11.60	5.33	6.71	9.95	11.37
4.0	1.0	2.5	0.2	5.41	6.77	9.86	11.47	5.29	6.65	9.88	12.51
4.0	1.0	3.0	0.2	5.53	6.85	9.90	11.55	5.41	6.56	9.96	11.50
4.0	1.0	2.0	0.1	5.45	6.79	9.85	11.49	5.35	6.69	10.04	11.42
4.0	1.0	2.0	0.3	5.41	6.91	10.21	11.71	5.43	6.78	9.95	11.47
4.0	1.0	2.0	0.4	5.36	6.78	9.89	11.73	5.27	6.67	10.10	11.34
4.0	1.0	2.0	0.5	5.29	6.84	10.16	11.63	5.35	6.70	10.12	11.59
4.0	1.0	2.0	0.6	5.40	6.85	11.12	11.65	5.40	6.78	9.95	11.53

Note: nu = [phen or terpy] $\times 10^3$ M and C = [**1**] or [**2**] or [**3**] or [**4**] $\times 10^5$ M.

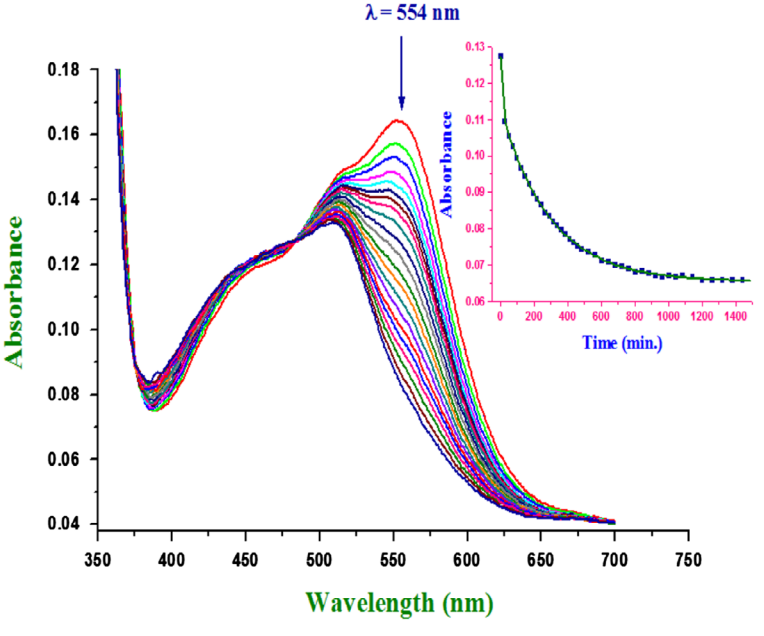

Figure 2. UV–vis spectral changes observed during the reaction between $[Fe(PDT)_2(bpy)]^{2+}$ and phen. Inset is a typical kinetic trace at 554 nm. $[[Fe(PDT)_2(bpy)]^{2+}] = 2.0\times10^{-5}$ M, [phen] = 1.0×10^{-3} M, pH = 4.0, μ = 0.2 M and temperature = 35°C.

2.5. Computational modeling

Computational modeling was performed by the Gaussian09 program package [25] to understand the structural and electronic differences of the investigated complexes [26, 27]. The geometry optimizations, frequency calculations, and mapped molecular orbital diagrams were carried out by means of density functional theory (DFT) using the B3LYP functional method [28–30]. The basis set 6–311 + G* for nitrogen, 6–31G* for carbon and hydrogen [31] and SDD for iron [32–35] were employed to get reliable results. The singlet state was used due to the low electronic spin of the polypyridyl iron(II) complexes. The complexes were computed with water as solvent, taking into account the solvolysis effects by means of the Conductor Polarizable Continuum Model (CPCM) [36–38]. All the structures were characterized as cationic species of formal charge 2+.

3. Results and discussion

Substitution reactions were carried out at 25, 35, and 45°C under *pseudo*-first-order conditions with [nu] ≫ [complex] and also within the pH range 3–6 in acetate buffers. The effect of concentration of complex and nu, pH, and ionic strength on the rate of substitution was studied. The k_{obs} values at 35°C are presented in table 2, while k_{obs} values at 25 and 45°C are given as Supplementary Data. The k_{obs} values depend directly on [nu] and inversely on pH. The plots of k_{obs} *versus* 1/[H$^+$] and k_{obs} *versus* [phen] were all linear and exemplary plots for the substitution of complex **1** by phen are given in figures 3(a) and 3(b), respectively, plots for the other reactions with phen and terpy are given as Supplementary Data. Ionic strength has no effect on reaction rate. Linear plots with positive slopes and large intercepts of k_{obs} *versus* [nu] and k_{obs} *versus* 1/[H$^+$] were observed. These observations suggest that these reactions proceed via two distinct paths, namely associative and dissociative.

3.1. Species distribution of the phen and terpy ligands

Phen is monobasic and exists as mono- and unprotonated forms whereas terpy is di-basic and exists as mono-, di-, and unprotonated forms in acidic media according to the following respective equilibria.

$$\text{phenH}^+ \underset{}{\overset{K_a}{\rightleftharpoons}} \text{phen} + \text{H}^+ \qquad (1)$$

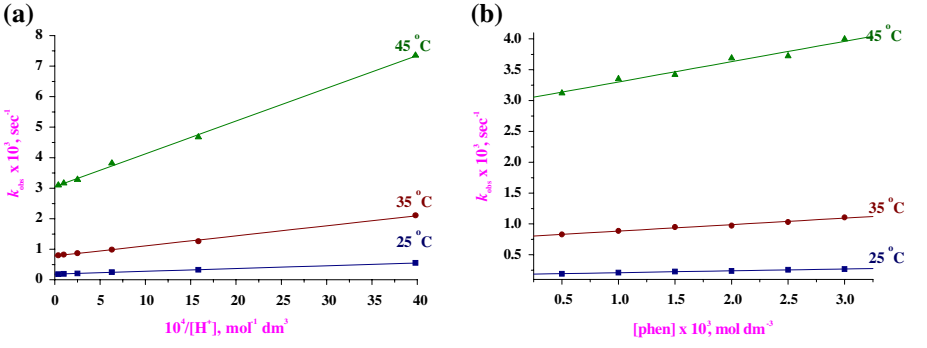

Figure 3. Linear plots of k_{obs} *vs.* (a) 1/[H$^+$] and (b) [phen] for the substitution of **1**, [[Fe(PDT)$_2$(bpy)]$^{2+}$] by phen. [[Fe(PDT)$_2$(bpy)]$^{2+}$] = 2.0×10^{-5} M, pH = 4.0 and μ = 0.2 M.

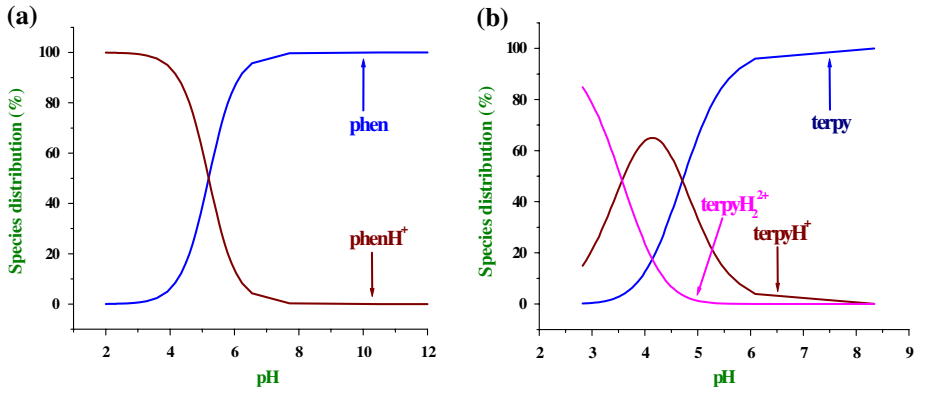

Figure 4. Species distribution curves of (a) phen and (b) terpy as a function of pH.

$$\text{terpyH}^{+} \underset{\rightleftharpoons}{K_{a_1}} \text{terpy} + \text{H}^{+} \tag{2}$$

$$\text{terpyH}_2^{+} \underset{\rightleftharpoons}{K_{a_2}} \text{terpyH}^{+} + \text{H}^{+} \tag{3}$$

Phen has a pK_a value of 5.02 [39] and terpy has pK_{a1} and pK_{a2} values of 3.57 and 4.71 [40] at K_{a_1} 25°C, respectively. Using these values, the percentage distribution of mono- and unprotonated forms of phen, mono-, and unprotonated and di-protonated forms of terpy have been computed in the pH range 2–10 using a simulation program [41]. The percentage distribution of phen and terpy with pH variation is shown in figures 4(a) and 4(b), respectively. The data used to plot are given as Supplementary Data.

From the species distribution curves, it is clear that the substituting ligands (phen or terpy) existed mostly in the mono-protonated form within the pH range considered for studying their substitution reactions with complexes **1**–**4**. However, the unprotonated forms of these nucleophiles are considered as the reactive species.

3.2. Proposed mechanism for the reaction of [Fe(PDT/ PPDT)$_2$(bpy)] (1 or 2) with phen

The reactions are first order with respect to concentration of complex. Ionic strength has no effect on rate of reaction which is an indication that the rate-limiting step involves the reaction between an ion and a neutral species or two neutral species. The k_{obs} values increase with increasing [nu] and decrease with increase in [H$^+$]. These observations suggest the following mechanistic paths.

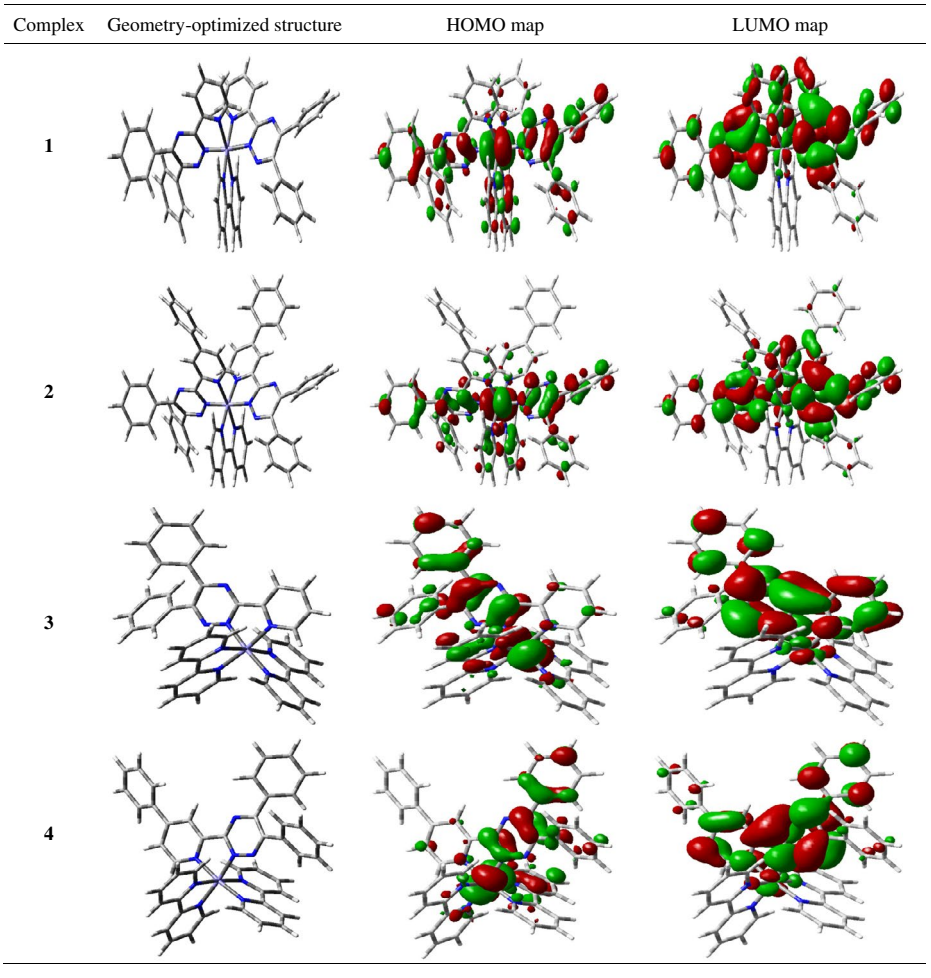

Figure 5. DFT-optimized frontier orbital energy structures, HOMO and LUMO maps for Fe(II) complexes at B3LYP/SDD level.

3.3. Dissociative path

Octahedral complexes generally undergo reversible dissociation. Thus, for the studied reactions, the formation of the five-coordinate intermediate, defined by the rate constant, k_1 to give the intermediate, [Fe(PDT/PPDT)(bpy)(PDT/PPDT-η^1)] is the rate-limiting step and hence the rate of substitution is independent of the incoming ligand. The five-coordinate complex reacts further with more phen molecules in a series of fast steps to give the final product $[Fe(phen)_3]^{2+}$. Detailed elementary reaction steps are given in Supplementary Data (equations 1–7).

The formation of the five-coordinate species [Fe(PDT/PPDT)(bpy)(PDT/PPDT-η^1)] is more likely than [$Fe(PDT/PPDT)_2$(bpy-η^1)]. Generally, in mixed-ligand complexes, the ligand which is more sterically hindered is likely to dissociate faster from the iron(II) center. Between the inert ligands PDT/PPDT or bpy, the PDT/PPDT is bulkier and offers more steric hindrance,

hence it is likely to dissociate from the iron(II) center to form a five-coordinate activated complex [Fe(PDT/PPDT)(bpy)(PDT/PPDT-η^1)].

3.4. Associative path

In this path, the incoming ligand (phen) coordinates to the iron(II) center to form a seven-coordinate intermediate $[Fe(PDT/PPDT)_2(bpy)(phen\text{-}\eta^1)]^{2+}$. Subsequently, the seven-coordinate intermediate rearranges itself and the phen molecule chelates to iron(II) center to form $[Fe(PDT/PPDT)(bpy)(phen)(PDT/PPDT\text{-}\eta^1)]^{2+}$. In a series of fast steps, $[Fe(PDT/PPDT)(bpy)(phen)]^{2+}$ reacts with more phen molecules to give the final product, $[Fe(phen)_3]^{2+}$ (elementary reaction steps are given as Supplementary Data equations 8–14).

3.5. Mechanism for reactions of [Fe(PDT/PPDT)(bpy)$_2$] (1 or 2) with terpy

The substitution of **1** or **2** with terpy is similar to what has been described for the substitution reactions of **1** or **2** with phen. The rate-determining step involved the formation of five- or seven-coordinate intermediates for the dissociative and associative paths as described in Supplementary Data equations 15–29. However, differences occur in the subsequent fast elementary steps due to the tridentate nature of the terpy ligand and its propensity to coordinate in a meridional fashion.

3.6. Mechanism for reactions of [Fe(PDT/PPDT)(bpy)$_2$] (3 or 4) with phen or terpy

The mechanism for the substitution of $[Fe(PDT/PPDT)(bpy)_2]$ (**3** or **4**) by phen or terpy follows a similar set of steps described above for **1** or **2** for both the dissociative or associative paths, respectively. The ultimate products are $[Fe(phen)_3]^{2+}$ and $[Fe(terpy)_2]^{2+}$ in the substitution of **3** or **4** by phen and terpy, respectively. The detailed mechanism for the substitution of **1**–**4** by phen and terpy is given as Supplementary Data equations 30–56. The substitution reactions of **1**–**4** with phen and terpy are summarized in scheme 2. Assuming that the two paths independently contributed to the rate, we can write the rate law:

$$\text{rate} = k_1[\text{complex}] + k_2[\text{complex}][\text{nu}]_e \tag{4}$$

As already stated, within the pH range for which the reaction were studied, the phen and terpy substituting ligands existed mostly in their mono-protonated forms. Therefore,

$$[\text{nu}]_t = [\text{Hnu}^+]_e + [\text{nu}]_e \tag{5}$$

Hence, from equilibrium equations (1)/(3),

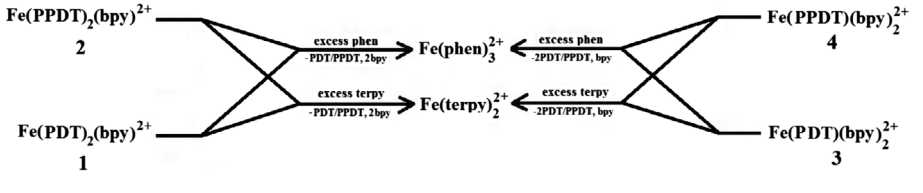

Scheme 2. A summary of the substitution reactions of complexes **1**–**4** with phen or terpy.

$$[Hnu^+]_e = \frac{[nu]_e[H^+]_e}{K_a} \tag{6}$$

therefore,

$$[nu]_e = \frac{K_a[nu]_t}{K_a + [H^+]_e} \tag{7}$$

$$\text{Rate} = k_1[\text{complex}] + \frac{k_2K_a[\text{complex}][nu]_t}{K_a + [H^+]_e} \tag{8}$$

$$\text{Rate} = [\text{complex}]\left\{k_1 + \frac{k_2K_a[nu]_t}{K_a + [H^+]_e}\right\} \tag{9}$$

the terms $[nu]_t$ and $[H^+]_e$ were replaced by [nu] and $[H^+]$ (initial concentrations of nu and H^+), respectively. Hence,

$$\text{Rate} = [\text{complex}]\left\{k_1 + \frac{k_2K_a[nu]}{K_a + [H^+]}\right\} \tag{10}$$

therefore,

$$k_{obs} = k_1 + \frac{k_2K_a[nu]}{K_a + [H^+]} \tag{11}$$

equation (11) can be modified to equation (12) by neglecting the term K_a, science $[H^+] \gg K_a$.

$$k_{obs} = k_1 + \frac{k_2K_a[nu]}{[H^+]} \tag{12}$$

Thus, plots of k_{obs} *versus* [nu] and $1/[H^+]$ are straight lines with positive slopes and intercepts. The specific second-order rate constant, k_2 for substituting the coordinated ligands by phen or terpy is obtained from the slope of a plot of k_{obs} *versus* [nu] (slope = $k_2K_a/[H^+]$) or k_{obs} *versus* $1/[H^+]$ (slope = $k_2K_a[nu]$). The intercept of either plot gives the first-order rate constant, k_1 for the overall dissociation process of the coordinated ligands from the Fe(II) complex. K_a values of phen or terpy at 25°C [39, 40, 42] were used to calculate the K_a values at higher temperatures (35 and 45°C) using the Perrin equation [43],

$$\frac{\Delta pK_a}{\Delta T} = \frac{pK_a - 0.9}{T} \tag{13}$$

where T is in Kelvin. Using the K_a values, the specific rate constants k_1 for the dissociative path and k_2 for the associative path at three different temperatures, the activation parameters such as E_a, $\Delta H^{\#}$, $\Delta S^{\#}$, and $\Delta G^{\#}$ for each path were computed from the Arrhenius and Eyring equations [44]. The specific rate constants and activation parameters are given in tables 3 and 4 for dissociative and associative paths, respectively.

In the associative path, the incoming ligand has a specific influence in the rate of reaction, which results in a difference in the k_2 values. It can be inferred from the above table that the specific rate constants for the substitution of the ligands from complexes **1**–**4** increase in the order **1**<**2**<**3**<**4**. The specific rate constants depend on the concentration of the entering polypyridyl ligand, signifying the formation of a new bond in the activated states of the reactions. Of the two nucleophiles, phen is the more reactive ligand due to its basicity usually expressed by the pK_a of the respective N-donor heterocyclic nucleophile [45–48]. The reactivity order of the nucleophiles is phen > terpy.

Generally, the substitution reactions at the iron(II) center occur via both dissociative and associative paths [49–51]. The relative magnitudes of the specific rate constants for the two paths indicate that the associative mode of activation dominates over the dissociative pathway through the rapid formation of a seven-coordinate intermediate in the rate determining step, which gives the final product in a series of fast steps [52, 53]. For the dissociative path, the values of k_1 are lower while the $\Delta H^{\#}$ values are higher. Further, $\Delta S^{\#}$ for the dissociative path is positive while it is negative for the associative path. Significantly negative entropy values indicate the formation of a highly ordered and more compact seven-coordinate activated complex in the associatively activated path [54–56]. The k_2, $\Delta H^{\#}$ or E_a, and $-\Delta S^{\#}$ values support the predominantly associative character of these reactions.

3.7. Computational analysis

Computational DFT calculations were performed in order to get an in-depth understanding of the structural as well the electronic differences of the complexes. Intrinsic descriptors such as ionization potential (I), electron affinity (A), chemical hardness (η), chemical softness (σ), chemical potential (μ), and dipole moment are helpful in explaining reactivity of the complexes investigated in the present study. The DFT-calculated geometry-optimized structures and frontier orbital energy (HOMO and LUMO) maps along with data are summarized in figure 5 and table 5, respectively. The DFT-calculated frontier-orbital diagrams show that most of the HOMO electron density is from the d-orbitals of the iron atom and partly from the conjugated π-molecular orbitals of the pyridyl rings in PDT/PPDT molecule. The LUMO electron density is primarily on the π-electron system of the ligand and a lower contribution from the d-orbitals on the Fe atom. For all the complexes, the HOMOs and LUMOs are on the π-electron system of the triazine ligands (PDT/PPDT) and d-orbitals of iron while bpy ligands do not have significant electron density.

From table 5, the bond lengths of Fe-N_{phen} are in the same order for all four complexes, indicating that the flow of electrons from phen to metal is uniform and the bpy ligand has no effect on the reactivity of the complexes. A similar conclusion has been drawn from the HOMO and LUMO maps of the complexes. Since the associative path predominates ($k_2 \approx 100k_1$ for all reactions), the DFT calculations will be discussed in support of an associative mechanism only.

Table 3. Specific rate constants and activation parameters for dissociative path of the reactions of **1**–**4** with phen and terpy.

	Dissociative path, $k_1 \times 10^3$, M s^{-1}							
	phen				terpy			
Temperature, °C / parameter	**1**	**2**	**3**	**4**	**1**	**2**	**3**	**4**
25	0.11 ± 0.02	0.14 ± 0.01	0.20 ± 0.01	0.22 ± 0.03	0.11 ± 0.02	0.13 ± 0.01	0.20 ± 0.02	0.23 ± 0.01
35	0.53 ± 0.02	0.66 ± 0.04	0.96 ± 0.05	1.10 ± 0.02	0.57 ± 0.04	0.60 ± 0.03	0.98 ± 0.05	1.15 ± 0.03
45	2.04 ± 0.04	2.73 ± 0.08	4.40 ± 0.08	5.10 ± 0.07	2.12 ± 0.09	2.60 ± 0.10	4.45 ± 0.08	5.17 ± 0.07
E_a, kJ mol^{-1}	115 ± 2	117 ± 1	121 ± 1	124 ± 3	114 ± 2	117 ± 1	120 ± 1	125 ± 2
$\Delta H^{\#}$, kJ mol^{-1}	112 ± 2	114 ± 1	119 ± 2	121 ± 2	113 ± 1	116 ± 3	118 ± 2	123 ± 2
$\Delta S^{\#}$, J K^{-1} mol^{-1}	57 ± 9	64 ± 11	82 ± 8	92 ± 7	55 ± 9	66 ± 8	83 ± 7	95 ± 10
$\Delta G^{\#}_{35°C}$, kJ mol^{-1}	95 ± 3	94 ± 2	93 ± 4	93 ± 3	97 ± 2	95 ± 3	97 ± 3	96 ± 2

Table 4. Specific rate constants and activation parameters for associative path of the reactions of **1**–**4** with phen and terpy.

	Associative path, $k_2 \times 10^1$, M s^{-1}							
	phen				terpy			
Temperature, °C / parameter	**1**	**2**	**3**	**4**	**1**	**2**	**3**	**4**
25	0.48 ± 0.02	0.68 ± 0.03	1.36 ± 0.04	2.07 ± 0.02	0.16 ± 0.03	0.25 ± 0.04	0.48 ± 0.05	0.68 ± 0.02
35	1.10 ± 0.05	1.49 ± 0.07	3.30 ± 0.04	4.50 ± 0.06	0.43 ± 0.04	0.56 ± 0.05	1.17 ± 0.08	1.51 ± 0.06
45	2.48 ± 0.08	3.17 ± 0.08	5.95 ± 0.10	7.94 ± 0.09	1.04 ± 0.07	1.34 ± 0.11	2.44 ± 0.13	3.04 ± 0.08
E_a, kJ mol^{-1}	65 ± 1	61 ± 2	58 ± 3	53 ± 1	73 ± 2	67 ± 4	61 ± 3	59 ± 2
$\Delta H^{\#}$, kJ mol^{-1}	62 ± 3	58 ± 1	56 ± 3	51 ± 4	71 ± 4	64 ± 1	58 ± 1	56 ± 2
$-\Delta S^{\#}$, J K^{-1} mol^{-1}	61 ± 11	72 ± 7	74 ± 9	88 ± 10	42 ± 8	62 ± 7	74 ± 13	78 ± 11
$\Delta G^{\#}_{35°C}$, kJ mol^{-1}	81 ± 2	80 ± 2	79 ± 4	78 ± 1	84 ± 3	83 ± 2	81 ± 3	80 ± 4

Table 5. DFT-calculated data for investigated complexes.

Complex	1	2	3	4
MO energy (eV)				
$I = -E_{HOMO}$	6.548	6.522	6.461	6.452
$A = -E_{LUMO}$	3.234	3.222	3.187	3.189
$\Delta E_{LUMO\text{-}HOMO}$	3.314	3.299	3.274	3.263
NBO charge				
Fe^{2+}	0.247	0.246	0.266	0.266
N_1 (= N_{phen})	−0.410	−0.410	−0.432	−0.432
N_2(= N_{phen})	−0.411	−0.411	−0.410	−0.410
N_3	−0.204	−0.203	−0.429	−0.428
N_4	−0.425	−0.428	−0.429	−0.429
N_5 (= $N_{pyridyl}$)	−0.424	−0.429	−0.424	−0.429
N_6(= $N_{triazine}$)	−0.204	−0.203	−0.204	−0.204
Bond lengths (Å)				
Fe-N_1 (Fe-N_{phen})	1.994	1.993	2.005	2.005
Fe-N_2 (Fe-N_{phen})	1.995	1.996	1.994	1.995
Fe-N_3	1.959	1.958	2.003	2.003
Fe-N_4	2.015	2.012	2.002	2.003
Fe-N_5 (Fe-$N_{pyridyl}$)	2.014	2.011	2.016	2.013
Fe-N_6 (Fe-$N_{triazine}$)	1.957	1.958	1.956	1.956
Chemical hardness (η)	1.657	1.650	1.637	1.632
Chemical softness (σ)	0.604	0.602	0.611	0.613
Electronegativity ($\chi = -\mu$)	4.891	4.872	4.824	4.821
Dipole moment (D)	2.298	4.373	11.982	12.324

NBO charge is a measure of π-electron delocalization and shows the degree of the aromaticity of the aromatic rings. Jaganyi and co-workers have reported the effect of the inert ligand on the rate of substitution at square planar Pt(II) complexes using natural bond order (NBO) charges on the metal centers [35, 57–61]. For associative substitution, high positive NBO charges on the metal center leads to high k_2 values. In table 5, complexes **1** and **2** have similar NBO charges on Fe^{2+} (0.247) which are significantly lower than those of complexes **3** and **4** (0.266). The lower NBO charges for complexes **1** and **2** are because the phenyl groups donate electrons into the triazine which decrease the NBO charges on the metal center depending on the number of coordinated triazine ligands. This reduces the π-acceptor ability of the triazine to receive electron density from the metal d-orbitals. The lower NBO charges on Fe^{2+} of complexes **3** or **4** slow down the rate of nucleophilic substitution by repelling the incoming nucleophile [62]. Additionally, in table 5, the Fe-$N_{triazine}$ bond length (~1.96 Å) is significantly shorter than the Fe-$N_{pyridyl}$ (~2.01 Å) and Fe-N_{phen} (~2.00 Å). This corroborates that the flow of electrons from the phenyl rings of triazine to the metal makes the Fe-$N_{triazine}$ bond shorter and stronger. Thus, phenyl groups on the coordinated triazine ring modulate the reactivity of the complexes.

The energy of the HOMO and LUMO is associated with the electron donating and accepting abilities of the inert ligands of the complexes, respectively [63]. Complexes with lower HOMO–LUMO energy gap are reactive and kinetically labile [64]. The HOMO–LUMO energy gap decreases from complex **1** to **4** as the reactivity increases. Electron descriptors [35, 65, 66] such as ionization potential (I), electron affinity (A) electro negativity (χ) = (I + A)/2, hardness (η)= (I–A)/2 and softness (σ) = 1/η, and dipole moment were calculated from the DFT data. Higher ionization potential or negative chemical potential energy, high chemical hardness (large HOMO-LUMO gap), and low softness (small HOMO-LUMO gap) values are observed for complex **1** compared to the rest. This complex is relatively more stable and

kinetically inert than the rest. The electron descriptors data for complexes **1**–**4** corroborates well with the order of reactivity **1**<**2**<**3**<**4**. The reactivity of complexes **1**–**4** has also a direct relationship with the dipole moment. The dipole moment increases with increase in polarizability or decrease in the HOMO-LUMO energy gap of the complexes [67–69]. Complex **1** has the lowest dipole moment (2.298) and **4** has the highest dipole moment (12.324) in line with the trend in the reactivity.

4. Conclusion

The substitution of mixed-ligand complexes **1**–**4** by phen or terpy occurs by both dissociative and associative mechanism. However, the higher k_2, lower $\Delta H^{\#}$, and significantly negative $\Delta S^{\#}$ values for the associative path clearly indicate that these substitution reactions proceeded predominantly by the associative mechanism. The phenyl groups on the triazine molecules increase the electron density on the triazine rings which are coordinated to the metal center via the nitrogen atoms. The inductive donation of electron density decreases the reactivity of the complexes from **1** to **4**. This is evidenced by a decrease in the NBO charge on Fe(II) that correlates with the phenyl groups of the coordinated triazine ligands. The reactivity order of the complexes is **1**<**2**<**3**<**4** and is well supported by trends in the DFT-calculated chemical reactivity descriptors such as the HOMO–LUMO gap, NBO charges on Fe^{2+}, η, χ, and dipole moments. The phen is a better incoming ligand than terpy, in line with the order of the basicity of the two nucleophiles.

Supplementary material

TOF-MS spectral data of complexes **1**–**4**, the observed pseudo-first-order rate constants (k_{obs}) values for the substitution of complexes **1**–**4** by phen and terpy at 25 and 45°C, UV–vis spectra, percentage of various species of phen and terpy in the pH range 3–6, straight line plots of k_{obs} *versus* $1/[H^+]$ and [phen] / [terpy], detailed mechanism for substitution of complexes **1**–**4** by phen and terpy are presented as Supplementary Data.

Acknowledgement

The authors are gratefully indebted to the University Grants Commission, New Delhi, India for awarding BSR fellowship and University of KwaZulu-Natal, South Africa for awarding post-doctoral fellowship to Rajesh Bellam.

Disclosure statement

No potential conflict of interest was reported by the authors.

Funding

This work was supported by the University of KwaZulu-Natal, South Africa; and the University Grands Commission, India.

References

[1] L.C. Kamra, G.H. Ayres. *Anal. Chim. Acta*, **78**, 423 (1975).
[2] L.L. Stookey. *Anal. Chem.*, **42**, 779 (1970).
[3] R. Steinhaus, D.W. Margerum. *J. Am. Chem. Soc.*, **88**, 441 (1966).
[4] M. Tubino, E.J. Vichi. *Inorg. Chim. Acta*, **28**, 29 (1978).
[5] J. Baxendale, P. George. *Trans. Faraday Soc.*, **46**, 736 (1950).
[6] F.H. Case. *J. Org. Chem.*, **30**, 931 (1965).
[7] C. Chriswell, A. Schilt. *Anal. Chem.*, **46**, 992 (1974).
[8] A.A. Schilt, P.J. Taylor. *Anal. Chem.*, **42**, 220 (1970).
[9] A.A. Schilt, W.C. Hoyle. *Anal. Chem.*, **39**, 114 (1967).
[10] A.A. Schilt. *Talanta*, **13**, 895 (1966).
[11] A.A. Schilt. *J. Am. Chem. Soc.*, **82**, 3000 (1960).
[12] P. Taylor, A. Schilt. *Inorg. Chim. Acta*, **5**, 691 (1971).
[13] J. Burgess, R.I. Haines. *J. Chem. Soc., Dalton Trans.*, 1447 (1978).
[14] W. Baker Jr., H. Bobonich. *Inorg. Chem.*, **2**, 1071 (1963).
[15] E. Múñoz, M.D.M. Graciani, R. Jiménez, A. Rodríguez, M.L. Moyá, F. Sánchez. *Int. J. Chem. Kinet.*, **26**, 299 (1994).
[16] R. Blake, K.J. White, E.A. Shute. *J. Biol. Chem.*, **266**, 19203 (1991).
[17] S. Balasubramanian. *Synth. React. Inorg. Met.-Org. Chem.*, **29**, 377 (1999).
[18] R. Kobetić, M. Denžić, B. Zimmermann, S. Rončević, G. Baranović. *J. Coord. Chem.*, **65**, 3433 (2012).
[19] K. Wijaya, N. Yoshioka, H. Inoue. *J. Inorg. Biochem.*, **94**, 263 (2003).
[20] K. Wijaya, E.T. Wahyuni, N. Yoshioka, H. Inoue. *Biophys. Chem.*, **121**, 44 (2006).
[21] N. Yoshioka, H. Inoue. *Transition Met. Chem.*, **24**, 210 (1999).
[22] M. Mudasir, K. Wijaya, E.T. Wahyuni, H. Inoue. *Ind. J. Chem.*, **4**, 174 (2010).
[23] C.R. Gibbs. *Anal. Chem.*, **48**, 1197 (1976).
[24] *Origin 7.5™ SRO, v7.5714 (B5714)*, Origin Lab Corporation, Northampton One, Roundhouse Plaza, Northampton, MA, 01060 USA (2003).
[25] Gaussian 09, Revision A.1, M.J. Frisch, G.W. Trucks, H.B. Schlegel, G.E. Scuseria, M.A. Robb, J.R. Cheeseman, G. Scalmani, V. Barone, B. Mennucci, G.A. Petersson, H. Nakatsuji, M. Caricato, X. Li, H.P. Hratchian, A.F. Izmaylov, J. Bloino, G. Zheng, J.L. Sonnenberg, M. Hada, M. Ehara, K. Toyota, R. Fukuda, J. Hasegawa, M. Ishida, T. Nakajima, Y. Honda, O. Kitao, H. Nakai, T. Vreven, J.A. Montgomery Jr., J.E. Peralta, F. Ogliaro, M. Bearpark, J.J. Heyd, E. Brothers, K.N. Kudin, V.N. Staroverov, R. Kobayashi, J. Normand, K. Raghavachari, A. Rendell, J.C. Burant, S.S. Iyengar, J. Tomasi, M. Cossi, N. Rega, J.M. Millam, M. Klene, J.E. Knox, J.B. Cross, V. Bakken, C. Adamo, J. Jaramillo, R. Gomperts, R.E. Stratmann, O. Yazyev, A.J. Austin, R. Cammi, C. Pomelli, J.W. Ochterski, R.L. Martin, K. Morokuma, V.G. Zakrzewski, G.A. Voth, P. Salvador, J.J. Dannenberg, S. Dapprich, A.D. Daniels, O. Farkas, J.B. Foresman, J.V. Ortiz, J. Cioslowski, D.J. Fox. *Gaussian Manual*, Gaussian Inc, Wallingford (2009).
[26] A.E. Reed, R.B. Weinstock, F. Weinhold. *J. Chem. Phys.*, **83**, 735 (1985).
[27] A.E. Reed, F. Weinhold. *J. Chem. Phys.*, **78**, 4066 (1983).
[28] A.D. Becke. *Phys Rev. A*, **38**, 3098 (1988).
[29] A.D. Becke. *J. Chem. Phys.*, **98**, 5648 (1993).
[30] C. Lee, W. Yang, R.G. Parr. *Phys. Rev. B*, **37**, 785 (1988).
[31] W.J. Hehre, R. Ditchfield, J.A. Pople. *J. Chem. Phys.*, **56**, 2257 (1972).
[32] P. Fuentealba, H. Preuss, H. Stoll, L. Von Szentpály. *Chem. Phys. Lett.*, **89**, 418 (1982).
[33] T.H. Dunning, P.J. Hay. In *Modern Theoretical Chemistry*, H.F. Schaefer (Ed.), Vol. 3, pp. 1–27, Plenum, New York (1977).
[34] W. Sameera, M. Hatanaka, T. Kitanosono, S. Kobayashi, K. Morokuma. *J. Am. Chem. Soc.*, **137**, 11085 (2015).
[35] R. Bellam, D. Jaganyi. *Int. J. Chem. Kinet.*, **49**, 182 (2017).
[36] V. Barone, M. Cossi. *J. Phys. Chem. A*, **102**, 1995 (1998).
[37] M. Cossi, N. Rega, G. Scalmani, V. Barone. *J. Comp. Chem.*, **24**, 669 (2003).
[38] Z. Chval, M. Sip, J.V. Burda. *J. Comp. Chem.*, **29**, 2370 (2008).
[39] P.G. Daniele, C. Rigano, S. Sammartano. *Talanta*, **32**, 78 (1985).

[40] W.W. Brandt, J.P. Wright. *J. Am. Chem. Soc.*, **76**, 3082 (1954).
[41] L. Alderighi, P. Gans, A. Ienco, D. Peters, A. Sabatini, A. Vacca. *Coord. Chem. Rev.*, **184**, 311 (1999).
[42] W.W. Brandt, F.P. Dwyer, E.D. Gyarfas. *Chem. Rev.*, **54**, 959 (1954).
[43] D. Perrin. *Aust. J. Chem.*, **17**, 484 (1964).
[44] M.G. Evans, M. Polanyi. *Trans. Faraday Soc.*, **31**, 875 (1935).
[45] B. Pitteri, G. Marangoni, L. Cattalini, F. Visentin, V. Bertolasi, P. Gilli. *Polyhedron*, **20**, 869 (2001).
[46] B. Pitteri, G. Marangoni, L. Cattalini. *J. Chem. Soc., Dalton Trans.*, 3539 (1994).
[47] Z.D. Bugarčić, B. Petrović, E. Zangrando. *Inorg. Chim. Acta*, **357**, 2650 (2004).
[48] B. Pitteri, M. Bortoluzzi. *Polyhedron*, **25**, 2698 (2006).
[49] E.R. Gardner, F.M. Mekhail, J. Burgess, J.M. Rankin. *J. Chem. Soc., Dalton Trans.*, 1340 (1973).
[50] J. Burgess. *J. Chem. Soc., Dalton Trans.*, 1061 (1972).
[51] D. Margerum, L. Morgenthaler. *J. Am. Chem. Soc.*, **84**, 706 (1962).
[52] J.A. Broomhead, F.P. Dwyer. *Aust. J. Chem.*, **14**, 250 (1961).
[53] F. Basolo, F.P. Dwyer. *J. Am. Chem. Soc.*, **76**, 1454 (1954).
[54] M. Tobe, J. Burgess. *Inorganic Reaction Mechanisms*, Addison Wesley Longman Addison Wesley Longman, Essex (1999).
[55] G. Visweswara Rao, Y. Sridhar, P.G. Hela, T. Padhi, N.R. Anipindi. *Transition Met. Chem.*, **24**, 566 (1999).
[56] R. Bellam, N.R. Anipindi. *Transition Met. Chem.*, **39**, 311 (2014).
[57] A. Shaira, D. Jaganyi. *J. Coord. Chem.*, **67**, 2843 (2014).
[58] I.M. Wekesa, D. Jaganyi. *J. Coord. Chem.*, **69**, 389 (2016).
[59] B.B. Khusi, A. Mambanda, D. Jaganyi. *Transition Met. Chem.*, **41**, 194 (2016).
[60] G. Kinunda, D. Jaganyi. *Transition Met. Chem.*, **39**, 939 (2014).
[61] V.E. Matulis, Y.S. Halauko, O.A. Ivashkevich, P.N. Gaponik. *J. Mol. Strucg.: THEOCHEM*, **909**, 19 (2009).
[62] R. Bellam, G.G. Raju, N.R. Anipindi, D. Jaganyi. *Transition Met. Chem.*, **41**, 271 (2016).
[63] A.Y. Musa, A.A.H. Kadhum, A.B. Mohamad, A.A.B. Rahoma, H. Mesmari. *J. Mol. Struct.*, **969**, 233 (2010).
[64] G. Gece, S. Bilgiç. *Corr. Sci.*, **51**, 1876 (2009).
[65] R.G. Parr, R.G. Pearson. *J. Am. Chem. Soc.*, **105**, 7512 (1983).
[66] R.G. Pearson. *Inorg. Chem.*, **27**, 734 (1988).
[67] P. Atkins, J. De Paula. *Physical Chemistry for the Life Sciences*, Oxford University Press, USA (2011).
[68] M.M. Islam, M.D.H. Bhuiyan, T. Bredow, A.C. Try. *Comp. Theor. Chem.*, **967**, 165 (2011).
[69] K. Parimala, V. Balachandran. *Spectrochim. Acta, Part A*, **81**, 711 (2011).